

Quantum phase transitions in heavy fermion metals and Kondo insulators

Qimiao Si^{*,1} and Silke Paschen^{*,2}

¹ Department of Physics and Astronomy, Rice University, Houston, Texas 77005, USA

² Institute of Solid State Physics, Vienna University of Technology, Wiedner Hauptstr. 8-10, 1040 Vienna, Austria

* Corresponding author: e-mail qmsi@rice.edu; paschen@ifp.tuwien.ac.at

Strongly correlated electron systems at the border of magnetism are of active current interest, particularly because the accompanying quantum criticality provides a route towards both strange-metal non-Fermi liquid behavior and unconventional superconductivity. Among the many important questions is whether the magnetism acts simply as a source of fluctuations in the textbook Landau framework, or instead serves as a proxy for some unexpected new physics. We put into this general context the recent developments on quantum phase transitions in antiferromagnetic heavy fermion metals. Among these are the extensive recent theoretical and experimental studies on the physics of Kondo destruction in a class

of beyond-Landau quantum critical points. Also discussed are the theoretical basis for a global phase diagram of antiferromagnetic heavy fermion metals, and the recent surge of materials suitable for studying this phase diagram. Furthermore, we address the generalization of this global phase diagram to the case of Kondo insulators, and consider the future prospect to study the interplay among Kondo coherence, magnetism and topological states. Finally, we touch upon related issues beyond the antiferromagnetic settings, arising in mixed valent, ferromagnetic, quadrupolar, or spin glass f -electron systems, as well as some general issues on emergent phases near quantum critical points.

Copyright line will be provided by the publisher

1 Introduction Electron correlations give rise to a variety of novel phenomena, including unconventional superconductivity and non-Fermi liquid behavior. Pertinent materials include cuprate and iron-based superconductors, heavy fermion metals and organic charge-transfer salts. In the presence of correlations, we face the central question of how the electrons are organized and, in particular, whether there are principles that are universal among the various classes of the strongly correlated materials. One such principle, which has come to the forefront in recent years, is quantum criticality [1,2].

A quantum critical point (QCP) arises at a second-order transition between two ground states. The distinct ground states themselves occur due to competing interactions of a many-body system. The collective fluctuations of the QCP control the physics of the quantum critical regime, which corresponds to a wide parameter range at non-zero temperature. While quantum criticality is of interest in its own right, and is being discussed in a variety of contexts ranging from insulating magnets to designer materials such as quantum dots and cold atom systems, it plays a special role in strongly correlated electron systems. Quantum critical-

ity provides a mechanism for both the non-Fermi liquid behavior and emergent phases such as unconventional superconductivity.

In this paper, we focus primarily on the issues arising in strongly correlated f -electron systems. These systems have been serving as a prototype setting to study the physics of quantum criticality. We will in particular highlight a class of QCPs in the antiferromagnetic (AF) Kondo lattice systems, which features the physics of Kondo destruction. The latter also gives rise to a global phase diagram, involving zero-temperature states that are distinct not only by the AF order but also by the nature of the Fermi surfaces. Experimental probes of such “beyond-Landau” QCPs and emergent phases are discussed. We also consider the analogous issues in Kondo insulators, extend the notion of Kondo destruction to mixed valent or ferromagnetic settings, and briefly discuss quantum criticality in quadrupolar and spin glass cases. Finally, we address several issues concerned with emergent phases around QCPs.

2 Local moments and competing interactions Heavy fermion systems represent canonical settings in

Copyright line will be provided by the publisher

which localized magnetic moments and itinerant conduction electrons coexist [3,4,5,6]. There are interactions not only among the local moments but also between the local moments and conduction electrons. The competition between these interactions gives rise to distinct ground states. Therefore, heavy fermion systems provide a fertile setting for quantum phase transitions.

The Kondo lattice Hamiltonian reads:

$$H_{\text{KL}} = \sum_{ij} t_{ij} c_{i\sigma}^\dagger c_{j\sigma} + \sum_{ij} I_{ij} \mathbf{S}_i \cdot \mathbf{S}_j + \sum_i J_K \mathbf{S}_i \cdot c_i^\dagger \frac{\boldsymbol{\sigma}}{2} c_i \quad (1)$$

It describes materials which contain spin- $\frac{1}{2}$ local moments (\mathbf{S}_i at every site i) that are physically associated with the localized f electrons, and a band of conduction electrons ($c_{i\sigma}$). The parameters t_{ij} and I_{ij} are respectively the hopping matrix of the conduction electrons (with bandwidth W) and the RKKY exchange interaction among the local moments (with a characteristic strength I), while J_K is the AF Kondo exchange interaction. We consider the simplest case, corresponding to one local moment per unit cell, and a filling of x conduction electrons per unit cell.

An effective single-ion Kondo energy scale T_0 signifies the onset of initial Kondo screening: the local moments are essentially decoupled from the conduction electrons at $T \gg T_0$, but develop dynamical singlet correlations with the conduction electrons as T is lowered towards T_0 . This provides a means to check the validity of the Kondo lattice Hamiltonian through measurements at temperatures above or around T_0 . Examples are the observation of Curie-Weiss behavior in the magnetic susceptibility, and a single-ion Kondo peak in the photoemission [7] and STM spectra [8].

As temperature is further lowered, the system may evolve towards different ground states. In one ground state, the local moments form a spin singlet with the conduction electrons. This Kondo entanglement turns each local moment into an electronic Kondo resonance excitation. The excitations occur at low energies, near the bare Fermi energy of the conduction electrons. These resonance excitations hybridize with the conduction electrons, forming renormalized quasiparticle bands that are separated by a hybridization gap [6].

For the generic case of incommensurate fillings with $x < 1$, the total electron count is $1 + x < 2$. Therefore, the Fermi energy will be in the lower hybridized band, located in the peak part of the DOS. This gives rise to a heavy Fermi liquid (FL) state with enhanced quasiparticle mass and a large Fermi surface.

In the special case of commensurate filling, $x = 1$, the total electron count is 2 per unit cell, corresponding to half-filling. The renormalized Fermi energy must be in the middle of the hybridization gap, leaving the lower hybridized band completely occupied and the upper one completely empty. The result is a Kondo insulator [9, 10, 11].

Ground states other than the Kondo entangled state are also possible. The local moments are coupled to each other through an exchange interaction. In Eq. (1), this is the RKKY interaction I ; up to Sect. 7, we will consider it to be AF. This exchange interaction promotes AF order. Correspondingly, the Kondo and RKKY interactions compete against each other [12, 13]. This competition is captured by the tuning parameter $\delta \equiv T_K^0/I$, where $T_K^0 \approx \rho_0^{-1} \exp(-1/\rho_0 J_K)$, with ρ_0 being the density of states of the conduction electrons at the Fermi energy, parameterizes the Kondo interaction.

In experiments, this tuning is accomplished by the application of external parameters. Typical examples are applying pressure, chemical substitution or magnetic field. Applying pressure increases/decreases δ in Ce/Yb-based heavy fermion compounds. Isoelectronic substitution of the ligands with smaller/larger atoms has the effect of applying positive/negative chemical pressure, although one needs to keep in mind that substitutions also introduce additional disorder. Finally, an external magnetic field influences the tendencies towards Kondo screening and AF order to different degrees (small magnetic fields reduce the Kondo scale in quadratic order but are coupled to the AF order linearly), thereby modifying the ratio δ .

The explicit observation of AF QCPs in several heavy fermion materials provides a setting to study quantum criticality in general. Furthermore, here, quantum criticality becomes intertwined with two of the key notions of correlated electrons: non-Fermi liquid behavior and, in many cases, unconventional superconductivity, occur in the quantum critical regime of heavy fermion metals.

3 Antiferromagnetic quantum critical points

Weak metallic antiferromagnets such as Cr are well-described in terms of a spin-density-wave (SDW) order. The order parameter is the staggered magnetization. Correspondingly, its transition at $T = 0$ to a paramagnetic metal phase is described by an SDW QCP [14, 15, 16]. This description falls into the Landau framework, with the order parameter differentiating between the phases and the fluctuations of the order parameter describing the quantum criticality.

Microscopically, this has been studied in terms of a one-band Hubbard model [14]. The SDW order is induced by the Coulomb repulsion, and the effective field theory is a quantum Ginzburg-Landau action [14],

$$\mathcal{S} = \int d\mathbf{q} \frac{1}{\beta} \sum_{i\omega_n} (r + c\mathbf{q}^2 + |\omega_n|/\Gamma_{\mathbf{q}}) \phi^2 + \int u \phi^4 + \dots (2)$$

which describes the fluctuations of the order parameter, ϕ , in both space (\mathbf{x}) and imaginary time (τ). This yields an effective dimensionality $d + z$, where d is the spatial dimension and z is the dynamic exponent. The wavevector \mathbf{q} and Matsubara frequency ω_n are reciprocal to \mathbf{x} and τ , respectively.

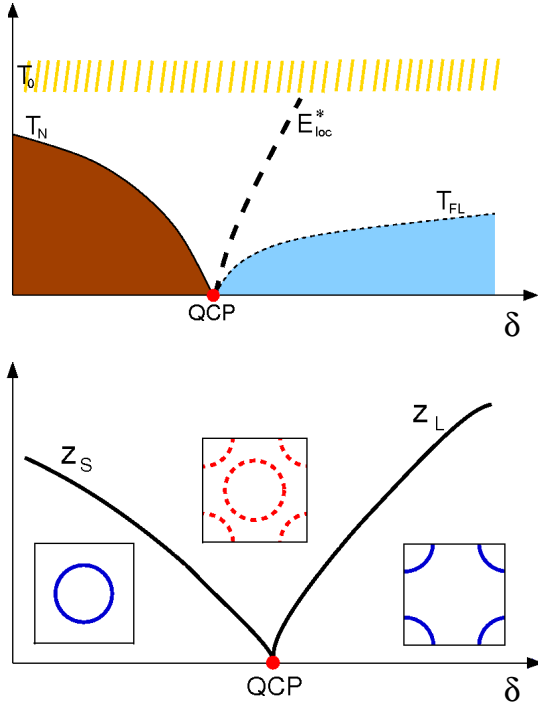


Figure 1 (top) Local quantum criticality is characterized by the collapse of an energy scale, E_{loc}^* , at the continuous onset of AF order. Here T_0 is a crossover temperature scale marking the initial onset of Kondo screening as temperature is lowered, and δ is the non-thermal tuning parameter representing the ratio of the bare Kondo scale to the RKKY interaction. T_N is the Néel transition temperature, and T_{FL} is the temperature scale for the heavy Fermi liquid state with a Kondo-entangled ground state. The QCP occurs at $\delta = \delta_c$. (bottom) Collapse of the quasiparticle residues across the local QCP. z_L and z_S are quasiparticle residues for the small (left inset) and large (right inset) Fermi surfaces, respectively. At the QCP, the quasiparticles are critical on both the small and large Fermi surfaces.

Theoretical studies on QCPs in AF heavy fermion metals have led to beyond-Landau QCPs, which feature inherently quantum modes besides the order-parameter fluctuations. While this notion extends to general contexts, for heavy fermion metals the emphasis has been on the critical modes associated with the destruction of the Kondo effect. Such critical modes are in addition to the fluctuations of the AF order parameter.

This Kondo destruction has provided insights into early puzzles on dynamical scaling in quantum critical heavy fermion systems, and led to predictions for the nature of Fermi surfaces and energy scales near the QCP that have been extensively observed in magnetotransport and quantum oscillation experiments.

3.1 Kondo destruction and beyond-Landau QCP

Heavy fermion metals are microscopically described in

terms of the Kondo lattice Hamiltonian, Eq. (1). Their traditional understanding invokes a ground state with a Kondo singlet between the local moments and conduction electrons. As described earlier, this Kondo entanglement in the ground state gives rise to an excitation spectrum with a Kondo resonance per local moment. The resulting heavy Fermi liquid state has a large Fermi surface, which incorporates $1 + x$ electrons per unit cell. In this way, the heavy quasiparticles near the Fermi energy can undergo an SDW order, thereby leading to an SDW QCP.

The dynamical spin correlations, however, may invalidate the very process that gives rise to the Kondo singlet ground state and the associated Kondo resonances. Such considerations have led to the notion of a local QCP, characterized by the physics of Kondo destruction. The phenomenon of Kondo destruction was already studied in the earlier renormalization-group (RG) study of the charge analogue of the dynamical RKKY vs Kondo competition [17], as well as its generalization to the spinful case [18, 19, 20]. Motivated by experiments on $\text{CeCu}_{5.9}\text{Au}_{0.1}$ [21], that we discuss in Sect. 3.3 below, concrete theoretical formulations for the Kondo destruction were advanced [22, 23, 24]. The theory implied the collapse of the extra energy scale E_{loc}^* , a jump of the Fermi energy across the QCP, and the critical nature of the quasiparticles on the whole Fermi surface at the QCP (cf. Fig. 1). The Kondo destruction was later also studied in a fermionic slave-particle representation of the Kondo lattice Hamiltonian [25, 26] and in dynamical mean field theory [27]. Finally, the notion of non-Fermi liquid quasiparticles on the whole Fermi surface (as opposed to only on the hot spots) has also been emphasized in a recent work based on a self-consistent method [28].

The extended dynamical-mean-field theory (EDMFT) [29, 30, 17] provides a means to study the weakening of the Kondo effect by the dynamical effects of RKKY interactions. The reduction of the Kondo singlet amplitude is described through the decrease of the energy scale E_{loc}^* .

At the local QCP, the Kondo destruction ($E_{loc}^* = 0$) occurs at δ_c , as shown in Fig. 1. In this case, the local spin susceptibility is

$$\chi(\mathbf{q}, \omega) = \frac{1}{f(\mathbf{q}) + A(-i\omega)^\alpha W(\omega/T)} \quad (3)$$

This form was derived with the aid of an ϵ -expansion RG approach [22, 24]. The exponent α has been found to be close to 0.75 (ranging from 0.72 to 0.83) [31, 32, 33].

The Kondo destruction implies that, as the QCP is approached from the paramagnetic side, the quasi-particle residue $z_L \propto (b^*)^2 \rightarrow 0$, where b^* is the strength of the pole of the conduction-electron self-energy $\Sigma(\mathbf{k}, \omega)$; this pole characterizes the Kondo resonance. In turn, electron excitations have a non-Fermi liquid form on the entire large Fermi surface.

3.2 Dynamical Kondo effect The breakdown of the large Fermi surface implies that the Fermi surface will be small on the antiferromagnetically ordered side. This is the

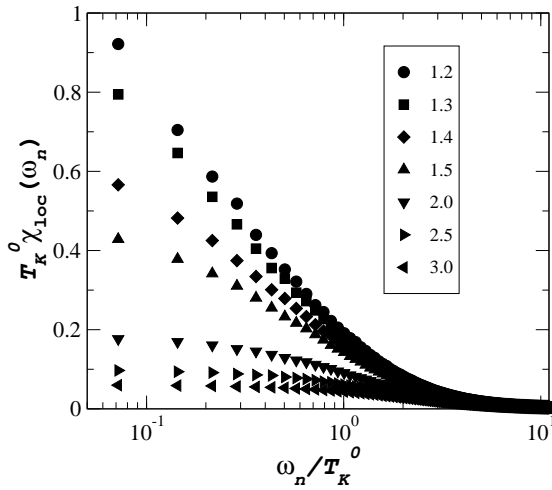


Figure 2 Dynamical Kondo effect inside the Kondo-destroyed AF phase. Shown is the normalized local susceptibility vs. Matsubara frequency, at a low temperature ($T \approx 0.01T_K^0$). The legend specifies I/T_K^0 . The gradual enhancement of the local dynamics as the QCP ($I_c/T_K^0 = 1.2$) is approached from the ordered side demonstrates the dynamical Kondo effect. Figure from Ref. [34].

AF_S phase, which will be further discussed in the next section. A dynamical Kondo effect will still generate a mass enhancement in the AF_S phase [34, 32, 33].

To consider this point further, the *static* amplitude of the Kondo singlet vanishes in the AF_S phase. Thus, the electron distribution function in the ground state displays a discontinuity at the small Fermi surfaces. By contrast, the effective mass is a dynamical quantity, measuring the dispersion of the Landau quasiparticles. The quasiparticle mass enhancement in the AF_S phase arises due to the *dynamical* part of the Kondo-singlet correlations, which persists in this phase. This has been explicitly demonstrated in the calculated local dynamics in the AF_S region of the Kondo lattice model [34, 32, 33], as illustrated in Fig. 2.

This dynamical Kondo effect ensures the continuity of the divergent effective mass as the QCP is approached from both the AF ordered side and the paramagnetic side.

3.3 Experimental probes of QCPs Numerous experimental techniques have been used to characterize quantum critical materials. Both temperature-dependent measurements at different fixed control parameter values and isothermal measurements as function of control parameter have been instrumental in advancing the field [4]. Temperature dependencies are frequently analysed by power law fits and then presented in terms of colour-coded temperature-tuning parameter phase diagrams, where the quantum critical region appears as a fan emerging from the QCP. Also insightful are scaling analyses. They test in which temperature range and up to which tuning-parameter

distance from the QCP the data can be collapsed onto a single universal curve, described by universal critical exponents. These critical exponents are then compared to theoretical predictions.

A milestone was the scaling analysis of the dynamical spin susceptibility of CeCu_{6-x}Au_x near the critical concentration $x_c = 0.1$, determined by inelastic neutron scattering at different energy transfers E [21]. The evidenced E/T scaling and the accompanying anomalous critical exponent of the SDW QCP, and have been interpreted in terms of Kondo destruction [22, 23].

Inelastic neutron scattering experiments on heavy fermion compounds are demanding as the typically small magnetic moments require large single crystalline samples and long data acquisition times. Therefore, such experiments have only been used to study a limited number of quantum critical heavy fermion metals; besides CeCu_{6-x}Au_x, these include the earlier results of Aronson et al. on UCu_{5-x}Pd_x [35] (which we will come back to in Sect. 7). Nevertheless, further progress was made by exploring materials with other experimental probes.

An important quantity is the Fermi surface. As it is expected to evolve qualitatively differently across an SDW and a local QCP [23, 24], probes to detect its evolution are of great interest. A simple measurement sensitive to changes of the Fermi surface is the Hall coefficient R_H . At $T = 0$, the Fermi surface is expected to evolve continuously across an SDW QCP but discontinuously, in the form of a jump, across a local QCP. The former is due to the order parameter increasing continuously as the ordered phase gets stabilized with increasing distance δ from the critical tuning parameter value δ_c . In the case of strong nesting, R_H may show a sizable (but continuous) evolution within the ordered phase. Across a local QCP, on the other hand, the Kondo entanglement is destroyed as the system orders. Thus, the $4f$ spins contribute to the Fermi surface only in the paramagnetic phase but drop out of the Fermi surface in the ordered phase. This leads to a jump of the Fermi surface. As the destruction of the Kondo entanglement is associated with an temperature scale T^* , that is in addition to the ordering temperature T_N and collapses with it only at the QCP, experimental signatures of the Kondo destruction are expected to occur away from $T_N(\delta)$ at finite temperatures. This is again in contrast to the SDW case, where $T_N(\delta)$ is the only temperature scale and thus the only place in the phase diagram where changes of the Fermi surface can be expected.

Of course, measurements of R_H can only be performed at finite temperatures. Thus, it is important to detect both the position (tuning parameter value at a given temperature) where a crossover in R_H is observed and the sharpness of the crossover (e.g. in the form of the full width at half maximum, FWHM). To distinguish between the two QCP scenarios, extrapolations of both quantities to $T = 0$ are needed. So far, this has been reliably done for both

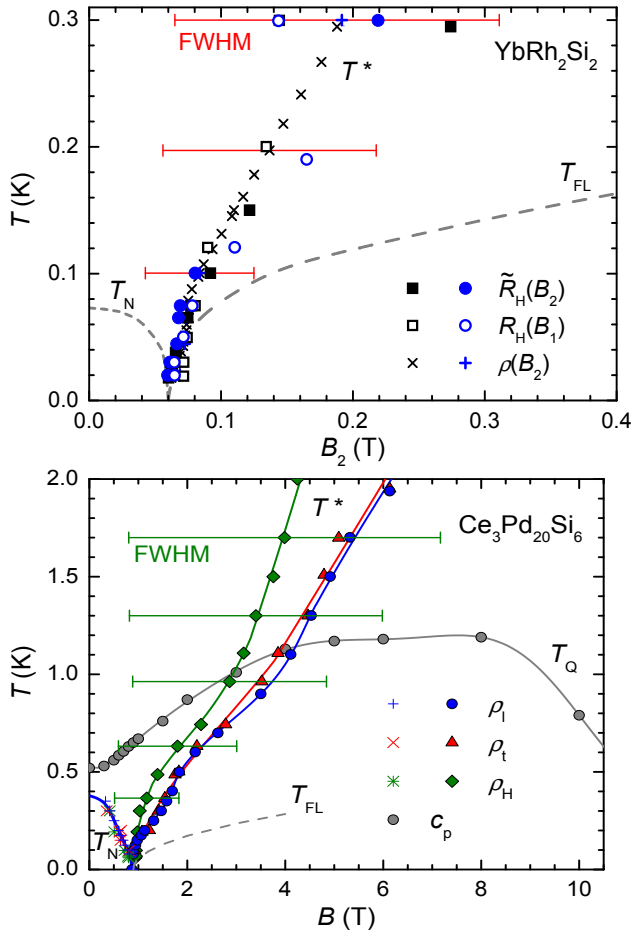


Figure 3 Temperature-magnetic field phase diagrams of YbRh_2Si_2 (top) and $\text{Ce}_3\text{Pd}_{20}\text{Si}_6$ (bottom), showing the Kondo breakdown scale T^* , the phase transition temperatures T_N and T_Q , and the temperature T_{FL} below which FL behaviour is recovered. The symbols indicate the measurements from which the characteristic temperatures were extracted. For YbRh_2Si_2 : Differential Hall coefficient $\tilde{R}_H(B_2)$ in a single-field experiment, Hall coefficient $R_H(B_1)$ in a crossed-field experiment, longitudinal resistivity $\rho(B_2)$; B_1 and B_2 are fields \parallel and \perp to the c axis. For $\text{Ce}_3\text{Pd}_{20}\text{Si}_6$: Longitudinal resistivity ρ_l , transverse resistivity ρ_t , Hall resistivity ρ_H and specific heat c_p , all in single field experiments. FWHM indicates the full width at half maximum of the crossover at T^* . In the extrapolation to $T = 0$, it collapses to zero for both materials. Figures adapted from [36,37].

YbRh_2Si_2 [38,36] and $\text{Ce}_3\text{Pd}_{20}\text{Si}_6$ [37]. In both systems, a crossover in R_H was observed across a scale T^* , that coincides with T_N only at the QCP. The FWHM of the crossover was shown to extrapolate to zero in the $T = 0$ limit (Fig. 3), thus evidencing the presence of a local QCP in both cases. (In $\text{Ce}_3\text{Pd}_{20}\text{Si}_6$, this occurs inside the ordered region of the phase diagram, see Fig. 3. This is fur-

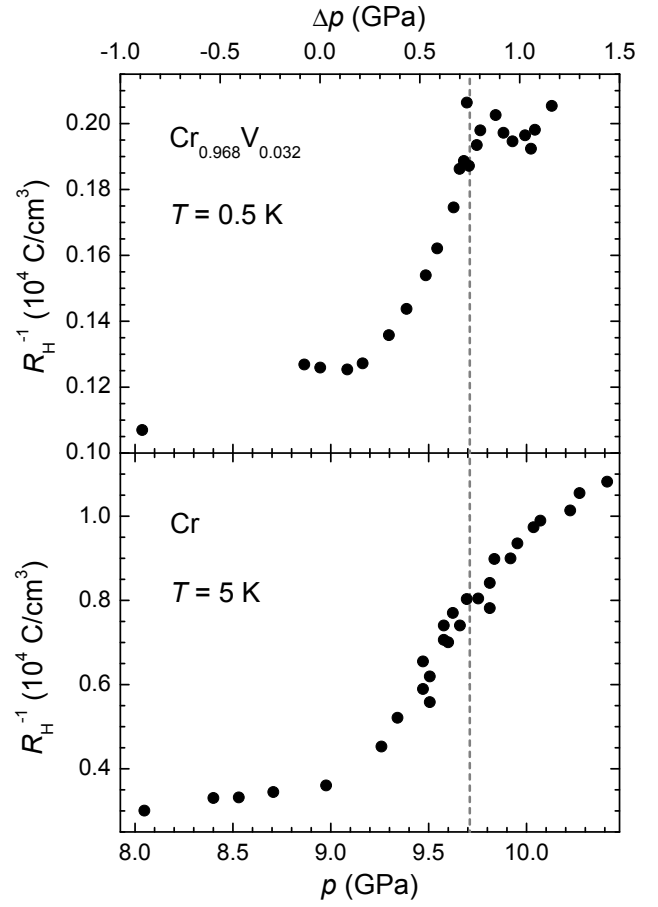


Figure 4 Evolution of the inverse Hall coefficient of $\text{Cr}_{1-x}\text{V}_x$ across its pressure-driven QCP. For $x = 0.032$ (top), tuning is done both by external and chemical pressure, for $x = 0$ (bottom) only external pressure was applied. The continuous evolution of $R_H^{-1}(p)$ confirms the absence of a jump in the Hall coefficient across an SDW QCP. Figures adapted from [39,40,41].

ther discussed in the next section.) By contrast, a combined hydrostatic and chemical pressure study of the itinerant antiferromagnet $\text{Cr}_{1-x}\text{V}_x$ revealed a continuous evolution of R_H across the SDW QCP, with a width of the drop of R_H^{-1} within the ordered phase below 9.7 GPa that is essentially independent of temperature (Fig. 4).

A second important tool to probe Fermi surface changes are de Haas-van Alphen (dHvA) experiments. These have been used to study the Fermi surface evolution of CeRhIn_5 as a function of pressure [42] at magnetic fields around 10 T, just above the upper critical field for the suppression of superconductivity H_{c2} .

In this material, the pressure-induced AF to non-magnetic quantum phase transition has been observed to be second order for fields above 3 T [43,44]. The second-order nature of this transition is further evidenced by the tendency of divergence near the critical pressure, p_c , for

both the cyclotron mass m^* [42] and the T^2 -resistivity coefficient A [45]. Across such an AF QCP, the dHvA frequencies undergo a sharp jump. In the AF ordered state, at $p < p_c$, they are compatible with the Fermi surface being small, while those in the paramagnetic state, at $p > p_c$, are consistent with the Fermi surface being large. Such a sudden jump of the Fermi surface across the QCP is again to be contrasted with the smooth evolution as indicated by the Hall-coefficient results across the SDW QCP in the Cr:V system.

We close this subsection by remarking on three aspects. First, as we discussed, the dynamical Kondo effect leads to mass enhancement in the AF_S phase. Within the local QCP description, this dynamical Kondo effect underlies the mass enhancement observed in the AF phases of $YbRh_2Si_2$, $CeCu_{6-x}Au_x$ and $CeRhIn_5$. Beyond these, recent experimental observations in the AF state of $CeIn_3$ at ambient pressure appear to provide evidence for a dynamical Kondo effect as well [46]. $CeCu_2Ge_2$, in its AF state, may also belong to AF_S , and a similar observation has also been reported recently [47].

Second, the critical destruction of quasiparticles at the QCP has recently been probed by thermal transport measurements in $YbRh_2Si_2$, which observed a violation of the Wiedemann-Franz law [48]. STM spectroscopy is also poised to probe the nature of the single-electron excitations in the quantum critical regime [49].

Third, recent inelastic neutron scattering measurements on $YbRh_2Si_2$ have finally observed the AF wavevector in the fluctuation spectrum at $T > T_N$ [50]. This is consistent with the order being AF, which has in the past been inferred from the facts that magnetic field applied in any direction reduces the ordering temperature and that the magnetic susceptibility is reduced below the ordering temperature. Unlike the size of the Fermi surface, the dynamical spin susceptibility *per se* does not unambiguously address the question of whether f electrons are localized or delocalized in the AF state. Still, the incommensurate wavevector is stable up to quite high energy, extending to as large as 1.25 meV, which is close to the (bare) Kondo energy scale; this would not be expected for an SDW order associated with the delocalized f electrons and appears to be more consistent with local-moment magnetism. It would be instructive to see how the AF wavevector may connect to the form of the RKKY interactions.

This neutron study opens the door to future measurements of the dynamical spin susceptibility of $YbRh_2Si_2$ at low frequencies and temperatures that may be able to address the nature of dynamical scaling in the quantum critical regime. In addition, at magnetic fields that correspond to the field-induced FL regime (Fig. 1, top), a resonance mode has been observed [50], which promises to shed light on the large-Fermi surface regime of the phase diagram.

4 Global phase diagram of antiferromagnetic heavy fermion metals

The notion of Kondo destruc-

tion not only provides a means to characterize novel QCPs but also opens up the possibility of new phases at zero temperature.

4.1 Theoretical basis A zero-temperature phase diagram has been proposed for the AF heavy fermion metals [51,52,53]. Figure 5(a), left panel, shows the two-parameter phase diagram. Here the horizontal axis is the Kondo coupling J_K , and the vertical axis G marks the quantum fluctuations of the local-moment magnetism; the latter is tuned by frustration and dimensionality.

The starting point of the theoretical basis is the establishment of AF_S , an antiferromagnetic phase with destruction of the Kondo effect and the concomitant small Fermi surface. The demonstration of its stability was based on an analysis of the Kondo lattice Hamiltonian in the $J_K \ll I \ll W$ limit. This limit allows an expansion around a new reference point, corresponding to $J_K = 0$, where the ordered local-moment system is decoupled from the non-interacting conduction electrons. With respect to this reference point, the effect of J_K can be systematically studied using a renormalization-group method. For the Ising case, the AF-ordered phase of the local-moment magnetism has a spin gap; as a result, J_K is irrelevant implying the stability of the AF_S phase [51].

For the case with full spin-rotational invariance, corresponding to an $SU(2)$ symmetry, the analysis is more involved. Using a quantum non-linear sigma model (QNL σ M) representation, and with the aid of a mixed gapless-boson-and-fermion RG method, the Kondo coupling is shown to be exactly marginal, leading to the stability of the AF_S phase [54].

A sufficiently large J_K gives rise to the Kondo entanglement, resulting in the standard heavy Fermi liquid state – a paramagnetic phase with a large Fermi surface. Therefore, AF_S and P_L represent two anchoring phases of the phase diagram in Fig. 5(a), left panel. The distinction between these two phases are beyond-Landau: in addition to the presence/absence of AF order, the two are also differentiated by the absence/presence of Kondo entanglement.

The global phase diagram features three types of transition sequences as the system goes from the AF_S phase to the P_L phase. The type I transition goes directly from AF_S to P_L , while the type II sequence corresponds to transitions from AF_S through AF_L to P_L . In other words, they differ in terms of whether the collapse of the Kondo effect occurs at the paramagnetic-to-AF QCP, or whether it is delayed until inside the ordered part of the phase diagram. This distinction was inferred from EDMFT studies [22, 24]. The AF_L phase corresponds to the SDW order of the heavy fermion quasiparticles of the P_L phase, and Kondo destruction occurs at the boundary between AF_L and AF_S phases. Note that, again, the dynamical Kondo effect in the AF_S phase ensures the continuity of the quasiparticle mass across its boundary with the AF_L phase.

The type III sequence from AF_S to P_L passes through P_S , a paramagnetic phase with Kondo destruction and

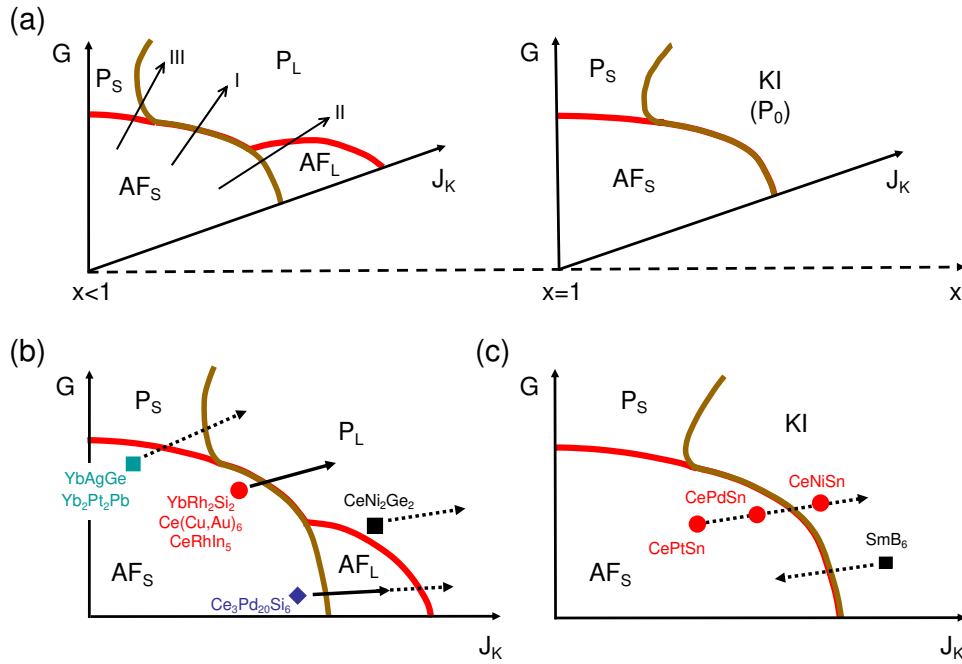


Figure 5 (a) Global phase diagram for heavy fermion metals (left) and Kondo insulators (right), linked by the tuning parameter conduction band filling x . G denotes the degree of quantum fluctuations of the local-moment magnetism, and J_K is the normalized Kondo coupling. The phases are differentiated by being paramagnetic (P) or antiferromagnetic (AF), with a large Fermi surface (L) which incorporates the f -electrons or a small Fermi surface (S) which does not. In the left panel, the three lines with arrow describe three trajectories of transitions from AF_S to P_L . In the right panel, the Kondo insulator (KI) phase, which is paramagnetic and has no Fermi surface (0) due to filled bands, replaces the P_L phase of the heavy fermion metal case; correspondingly, there exists no AF_L phase. Also shown are materials in the global phase diagrams for heavy fermion metals (b) and Kondo insulators (c).

hence small Fermi surface. The existence of the P_S phase can be seen by noting that increasing G of the local-moment magnetism alone (along the vertical axis) suppresses AF order. In the most typical cases, this leads to spin-Peierls order, which contains a spin gap. This spin gap renders a small J_K coupling to be irrelevant in the RG sense, thereby yielding the stability of a P_S phase. The competition between the P_L and P_S phase has been analyzed through the effect of the Berry phase in the QNL σ M representation [55].

4.2 Materials basis In Sect. 3.3, we have discussed the evidence for a quantum phase transition along the trajectory I (AF_S directly to P_L) in pure $YbRh_2Si_2$ as a function of the magnetic field, in $CeCu_{6-x}Au_x$ as a function of the substitution level x or pressure, and in $CeRhIn_5$ as a function of pressure at magnetic fields just above H_{c2} . These three cases are illustrated in Fig. 5(b).

Systematic investigations have also been performed on substituted and pressurized $YbRh_2Si_2$ [56, 57, 58, 59]. The resulting substitution level–magnetic field phase diagram is consistent with the profile of the global phase diagram in Fig. 5(b). In particular, compounds with Ni- and slight Ir-substitution for Rh also undergo a type I transition (AF_S

to P_L). For the case of Co-substitution for Rh as well as for the pure $YbRh_2Si_2$ under sufficient pressure, the transition appears to be divided into two stages, as along the type II trajectory with the Kondo destruction occurring inside the AF order. By contrast, for substitutions with Ge, or Ir concentrations beyond 2.5%, the transition seems to be of type III, a trajectory with the Kondo destruction outside the ordered phase. Direct measurements of the Kondo destruction in substituted and pressurized $YbRh_2Si_2$ remain, however, to be carried out.

To explore the global phase diagram, it is essential to broaden both the materials basis and the microscopic parameter variety. In particular, it is instructive to consider materials that lie in different ranges of the parameter G , the degree of quantum fluctuations in the local-moment magnetism. A recent investigation of the cubic compound $Ce_3Pd_{20}Si_6$ [37] probed the lower part of the global phase diagram, where G is small (dimensionality high) because of the absence of crystal anisotropy. A magnetic field-tuned QCP was observed to be accompanied by Kondo destruction. However, the phase above the critical field (cf. Fig. 3) still possess some kind of order. While both the type of order and the nature of the transition to the paramagnetic

phase need to be explored in future experiments, these results provide strong evidence for a type II trajectory.

In another cubic material, CeIn₃, dHvA experiments revealed a strong enhancement of the effective mass at a critical field within the ordered portion of the temperature–magnetic field phase diagram [60]. Thus, one may speculate that a type II trajectory is followed also by this material. In order to further test the global phase diagram, the role of dimensionality might also be studied more systematically, e.g. by the variation of the thickness of thin films of heavy fermion compounds. That such tuning might, in fact, be technically feasible was demonstrated by recent investigations on molecular beam epitaxy grown superlattices [61,62].

Geometrical frustration is expected to be a means to enhance G and reach the upper portion of the global phase diagram. Earlier studies considered the hexagonal YbAgGe [63]. More recently, Yb₂Pt₂Pb was investigated [64], in which the Yb moments are located on a quasi-two-dimensional Shastry-Sutherland lattice. In both cases, there exists an intermediate magnetic field regime between an AF order and a paramagnetic Fermi liquid regime, as illustrated in Fig. 5(b). Other materials in this category might be the fcc YbPtBi [65] and CePdAl with a distorted Kagome lattice [66].

Clearly, this is a subject that will see major developments in the near future, both theoretically and experimentally. These studies may ultimately lead us towards a classification of universality classes in quantum critical heavy fermions.

5 From local moment to mixed valent regime The Kondo lattice Hamiltonian is only valid when the underlying f -electron orbital is half-filled, with $n_f = 1$ per unit cell. Most of the heavy fermion metals displaying AF QCPs, such as YbRh₂Si₂ and CeCu_{6-x}Au_x, show a very large mass enhancement and a small Kondo temperature on the order of 10 K, and should therefore be in the Kondo limit. This is also expected to be the case for CeRhIn₅, for which the Kondo temperature is similarly about 10 K [67]. However, some materials do not appear to be in this limit. For instance, in the quantum critical superconductor β -YbAlB₄, the mass enhancement is modest, the Kondo temperature is rather high (on the order of 200 K), and the Yb valence was shown to be 2.75 (distinctly smaller than the integer valence 3) by hard X-ray photoemission spectroscopy [68]. While the occurrence of mixed valence is rare in heavy fermion metals, it is more common in Kondo insulators. In fact, these latter were originally referred to as mixed valent semiconductors [69]. For the prototypical Kondo insulator SmB₆ [70], mixed valence was detected early on [71]. Thus, it is interesting to look at the generalization of the Kondo lattice Hamiltonian to the mixed valent regime, where $n_f \neq 1$.

5.1 Periodic Anderson Model The underlying microscopic Hamiltonian in the mixed valent regime is the

periodic Anderson model

$$H_{\text{PAM}} = \sum_{\mathbf{k}\sigma} \epsilon_{\mathbf{k}} c_{\mathbf{k}\sigma}^\dagger c_{\mathbf{k}\sigma} + \sum_{\mathbf{k}\sigma} (V_{\mathbf{k}} f_{\mathbf{k}\sigma}^\dagger c_{\mathbf{k}\sigma} + \text{H.C.}) + \epsilon_f \sum_i n_{f,i} + U \sum_i n_{f,i\uparrow} n_{f,i\downarrow}, \quad (4)$$

which contains both spin and charge (valence) degrees of freedom of the f electrons. Here, $n_{f,i\sigma} = f_{i\sigma}^\dagger f_{i\sigma}$ and $n_{f,i} = \sum_{\sigma} n_{f,i\sigma}$.

Away from the local-moment limit, the inter-orbital Coulomb interaction

$$U_{fc} \sum_i n_{f,i} n_{c,i}, \quad (5)$$

that was introduced early on [72,13], also has to be considered. In the mixed valent regime, it influences the charge Kondo effect and the corresponding mixed valent non-Fermi liquid behavior [73,74,75].

5.2 Gaussian fixed point: generalization of the SDW QCP to mixed valence In the Kondo lattice case, assuming a finite Kondo energy scale at the QCP led to the description of the SDW QCP (Sect. 3.1). This description has been generalized to the mixed valence setting [76]. Microscopically, for U_{fc} below a critical value U_c , there is a valence crossover (n_f varies continuously with ϵ_f), whereas for $U_{fc} > U_c$ there is a first order valence transition (n_f shows a discontinuous decrease at some ϵ_f). The quantum-critical end point is a Gaussian fixed point, representing the generalization of the SDW QCP to the co-existing spin and charge sector. Indeed, the effective field theory of Ref. [76] has the form of the Hertz action, Eq. (2), with the damping $\Gamma_{\mathbf{q}} \propto q$ corresponding to a dynamic exponent $z = 3$. The QCP retains the generic feature of a Gaussian fixed point, in that ω/T scaling is violated; presumably H/T scaling is correspondingly violated as well.

Like in the SDW QCP, there will be no jump of the Fermi surface across such a QCP. Indeed, in order to realize a jump in the Fermi surface (and the Hall coefficient) in this picture, the transition is taken to be first order [77]. Alternatively, it was suggested that a jump in the Fermi surface can arise in a continuous transition due to folding of the large Fermi surface by the AF order [78]. This, however, appears incorrect: as the example of Cr:V (Fig. 4) demonstrated, the Hall coefficient must be continuous across such a QCP.

5.3 Interacting fixed point: generalization of the Kondo destruction to mixed valence To search for an interacting fixed point, it is important to address whether the Kondo destruction effect can still take place under the mixed valence condition. This is a delicate issue. In the Kondo lattice case, Kondo destruction amounts to the localization of f electrons. This is physically transparent, because localization can readily arise for a commensurate filling of an electronic orbital (one f electron per site). At

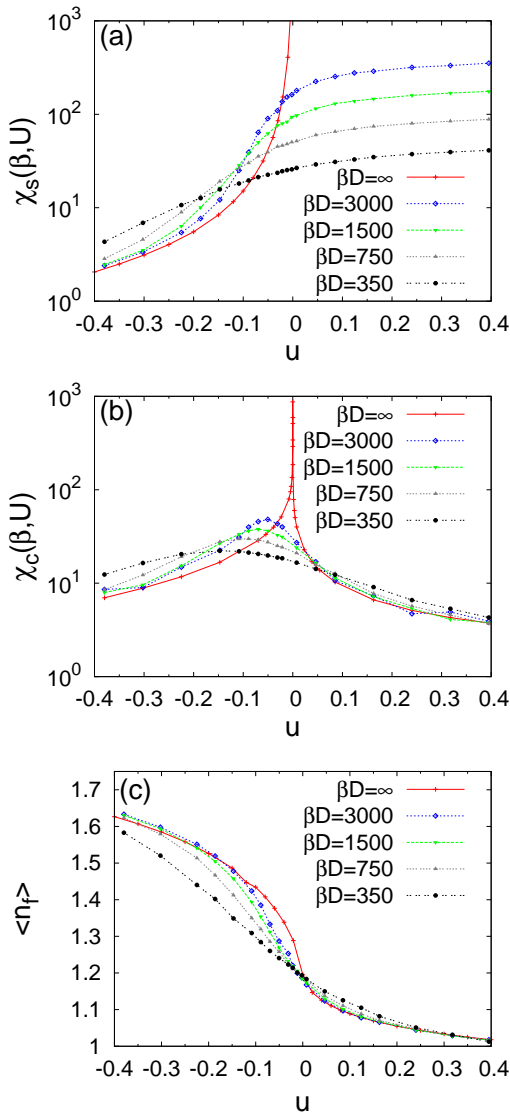


Figure 6 Kondo destruction in a mixed valence model. (a) Local static spin susceptibility χ_s vs. the tuning parameter $u = U/U_c - 1$ at various temperatures $T = 1/\beta$, measured in units of the half-bandwidth D ; its divergence on approaching the QCP ($u = 0$) at $T = 0$ signifies the Kondo destruction, with an associated Kondo energy scale in the spin sector going to zero as the QCP is approached from the Kondo-screened side. (b) Local static charge susceptibility χ_c is also divergent at the QCP. (c) Occupancy $\langle n_f \rangle$ vs the control parameter; at the QCP, $\langle n_f \rangle \neq 1$. Figures from Ref. [79].

mixed valence, the f orbital has a fractional, generally incommensurate, per-site occupancy; there is no mechanism known for electron localization in such cases.

This issue has recently been studied in a simplified setting, the pseudo-gapped particle-hole-asymmetric Ander-

son impurity model. It was shown that Kondo destruction occurs even at mixed valence [79], see Fig. 6. The physics in the spin sector is very similar to that for the local-moment case $n_f = 1$, in that an energy scale collapses as the QCP is approached from the Kondo-screened side. At the QCP, the charge fluctuations are singular along with the spin fluctuations. (This is in contrast to the particle-hole symmetric local-moment case $n_f = 1$, where the singular charge fluctuations are absent.) In line with the interacting nature of the fixed point, both the charge and spin responses display a magnetic field over temperature (H/T) and frequency over temperature (ω/T) scaling. When the results are generalized to the lattice case, the Kondo scale going to zero would imply that the Fermi surface jumps.

Recent measurements on the mixed valent heavy fermion compound β -YbAlB₄ have shown that the static magnetization exhibits H/T scaling [82,83], providing evidence for the interacting nature of an underlying QCP. The above theoretical study in a simplified model provides an existence proof of a local QCP at mixed valence with this kind of scaling behavior. If the QCP displays universality, such scaling behavior would also be expected at other mixed valent QCPs with Kondo destruction, irrespective of the microscopic details that give rise to valence fluctuations.

The theoretical results also suggest that, by restraining our further discussion to the Kondo case $n_f = 1$, we do not lose generality.

6 Global phase diagram of Kondo insulators In the case of half-filling, i.e. $x = 1$, the competition between the Kondo and RKKY interactions continues to operate. This case presents an opportunity to study a variety of correlated insulator states.

6.1 Global phase diagram As discussed in Sect. 2, when Kondo entanglement takes place, the ground state for the case of half-filling is a paramagnetic insulator, the Kondo insulator. Thus, in the global phase diagram, instead of a heavy fermion metal state with a large Fermi surface (P_L) we now have a state with no Fermi surface at all (P_0). Both the AF_S and P_S phases are expected to remain stable in the case of half-filling [84] (Fig. 5(a), right panel).

There is evidence that transitions between these phases can indeed be realized experimentally. While tuning through a QCP appears to be accomplished in a number of materials as function of magnetic field [85,86] or doping [87,88,89,90], we focus here on the conceptually simpler situation of tuning by external or chemical pressure. As an example, SmB₆ is tuned by pressure from the Kondo-insulating phase P_0 to an AF phase [91]. The dashed arrow in Fig. 5(c) suggests that this transition is to the phase AF_S . The explicit experimental demonstration that the AF phase of SmB₆ has a small Fermi surface is, however, still missing.

While most Kondo insulators are cubic, there are also a few representatives with lower crystalline symmetry,

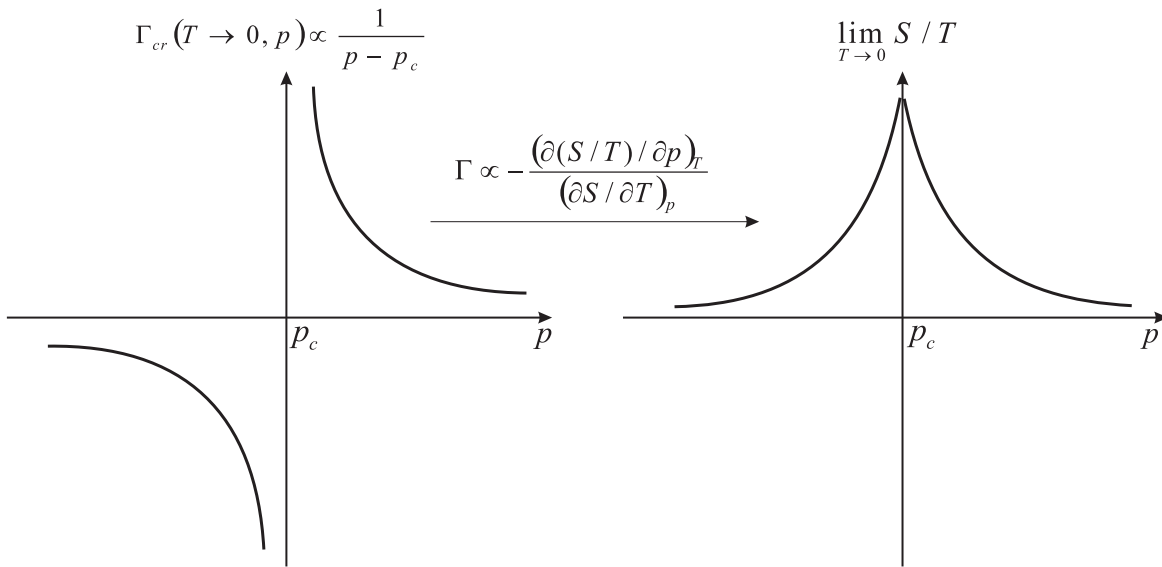


Figure 7 Entropy accumulation near QCP and divergence of the Grüneisen ratio, both of which follow from the scaling form of the free energy [80]. Figure from Ref. [81].

the most prominent one being orthorhombic CeNiSn. The isostructural and isoelectronic compounds CePtSn and CePdSn both order antiferromagnetically at low temperatures [92,93,94]. Transitions between the AF phase and the Kondo-insulating phase have been investigated both by chemical and by hydrostatic pressure tuning. The former has been realized by isoelectronic substitutions, i.e. in Ce(Pt_{1-x}Ni_x)Sn [95,96,88] or Ce(Pd_{1-x}Ni_x)Sn [97], and by hydrogenation [98]. Tuning by hydrostatic pressure appears more challenging. The magnetic order in CePdSn was shown to be suppressed only by hydrostatic pressure above 60 kbar [99]. A pressure of 20 kbar applied to CePtSn reduces the Néel temperature only slightly [100]. The ensemble of these experiments is represented schematically in Fig. 5(c) by the dashed arrow through CePtSn, CePdSn and CeNiSn. As for SmB₆, an explicit demonstration of a small Fermi surface AF_S in the antiferromagnetically ordered state still needs to be done. The lower symmetry of CeNiSn compared to SmB₆ is represented in Fig. 5(c) by placing CeNiSn and its relatives at a higher G value than pressure tuned SmB₆.

It would be instructive to consider other Kondo insulator systems in the context of the global phase diagram. For instance, CeRu₂Al₁₀ and CeFe₂Al₁₀ [101] might fit into this framework as well.

6.2 Correlated topological insulators and their interplay with Kondo coherence and magnetism In recent years, spin-orbit coupling in band insulators has been extensively studied as giving rise to topological insulators [102,103]. These bulk insulators have gapless helical surface states. In Kondo insulators, topological insulating states have been studied either through the spin-orbit coupling as manifested in the hybridization matrix [104] or

in conjunction with the spin-orbit coupling of the conduction electrons [105]. As such, Kondo insulators present an opportune system to study the interplay between topological and Kondo/magnetic effects, and even unconventional superconductivity near such boundaries. Recent measurements of several groups in SmB₆ have provided tentative evidence for the surface states of a topological insulator [106,107]. The evolution of such surface states under pressure [cf. Fig. 5(c)] represents an intriguing issue for future studies.

From the perspective of topological states [105], it is instructive to note that the $5d$ electrons of CePtSn will contain a large spin-orbit coupling, which may influence the topological nature of its expected insulating state at high pressure.

7 QCPs in other degrees of freedom

7.1 Weak ferromagnets and ferromagnetic heavy fermion metals Based on the field theory of Hertz for the ferromagnetic case, Eq. (2), the coupling to the fermions near the Fermi surface has been shown to yield non-analyticity in the coupling constants [108]. This is believed to turn the $T = 0$ transition first order, creating a “fish-tail” structure in the temperature–pressure–magnetic field phase diagram [109].

In Kondo lattice systems, the effect of local moments must be considered. For the ferromagnetic Kondo lattice, Ref. [110] studied the ordered phase using the QNL σ M basis (generalizing the study for the AF ordered phase mentioned in Sect. 4.1). Inside the ferromagnetic phase, the Fermi surface is small. The existence of this F_S phase raises the prospect that the $T = 0$ ferromagnetic to paramagnetic transition may also come in different varieties, in

a way that is analogous to the global phase diagram of the AF heavy fermion metals described earlier. In particular, this raises the intriguing possibility for a QCP in ferromagnetic heavy fermion metals.

The early dHvA measurements [111] in the ferromagnetic compound CeRu_2Ge_2 (with a Curie temperature $T_c = 8\text{ K}$) can be interpreted in terms of the F_S phase. Other ferromagnetic heavy fermion compounds of interest include the Re-doped URu_2Si_2 [112], $\text{CeRu}_2\text{Al}_2\text{B}$ [113], and YbNi_3Al_9 [114]. Recent experiments have provided evidence for a ferromagnetic QCP, both in YbNi_4P_2 [115] and in the iron pnictide $\text{Ce}(\text{Ru}_{1-x}\text{Fe}_x)\text{PO}$ [116].

7.2 Other degrees of freedom Quadrupolar order has also been discussed in the context of quantum criticality in a number of heavy fermion compounds. In the filled skutterudite $\text{PrOs}_4\text{Sb}_{12}$, antiferroquadrupolar order is believed to characterize a high-field ordered phase (HFOP), that is adjacent to a superconducting phase [117]. Thus, the possibility arises that the superconductivity in $\text{PrOs}_4\text{Sb}_{12}$ is driven by quantum critical fluctuations of quadrupolar degrees of freedom. In UPd_3 antiferroquadrupolar order can be weakened by small amounts of Np. At 5% doping, where the order is just suppressed, unconventional properties are observed, implicating a potential QCP [118].

$\text{UCu}_{5-x}\text{Pd}_x$ is the earliest system in which a dynamical spin susceptibility with an anomalous critical exponent and E/T scaling was discovered [35]. There have been theoretical studies which attributed this behavior to the effects of disorder, including a distribution of Kondo temperature scales [119] or a Griffiths phase [120]. However, it could also result from an interacting spin-glass QCP with Kondo destruction [51], that appears to occur in $\text{Sc}_{1-x}\text{U}_x\text{Pd}_3$.

8 Novel phases near quantum critical points

QCPs tend to nucleate new phases, as illustrated by the observation of superconductivity near heavy fermion QCPs [121]. From a macroscopic perspective, general scaling considerations show that entropy is maximized near a QCP [80,81]. This is illustrated in Fig. 7. Such an accumulation of entropy has been explicitly demonstrated across the field-induced metamagnetic QCP in $\text{Sr}_3\text{Ru}_2\text{O}_7$ [122]. An enhanced entropy suggests that the system is particularly prone to developing new order. In the global phase diagram, we may consider AF_L and P_S as new phases that emerge in the vicinity of QCPs. Another instructive case is provided by CeAgSb_2 , which possesses ferromagnetic order below about 10 K at ambient pressure. A pressure of about 3 GPa reduces the Curie temperature to about 4 K. Before the ferromagnetic order is completely suppressed, however, it succumbs to an AF state [123]. In other words, the AF state emerges at the border of a ferromagnetic order.

Of course, the most striking example is superconductivity developing near AF QCPs. We have discussed the strong evidence that the AF quantum phase transition in

CeRhIn_5 is described by a local QCP. A superconducting state of a very large T_c (when measured against the Kondo temperature) in CeRhIn_5 [67] occurs in the vicinity of its AF QCP [43,44]. Hence, this material provides a striking example for superconductivity that is driven by Kondo destruction, developing from a normal state with fluctuating Fermi surfaces and critical quasiparticles.

In the case of CeCu_2Si_2 , there is evidence that the asymptotic low-energy quantum critical behavior is of the SDW type. Nonetheless, the exchange energy gain is much larger than the condensation energy, which has been interpreted [124,125] in terms of a Kondo-destruction energy scale that is nonzero but relatively small compared to the Kondo scale. This suggests that Kondo destruction physics is part of the dynamics that drives superconductivity in CeCu_2Si_2 .

9 Summary and outlook We close with some perspectives and outlook.

The study of Kondo destruction and local quantum criticality has broad implications. The notion that quasiparticles break down over the entire Fermi surface represents a drastic departure from the traditional SDW description of an antiferromagnetic quantum critical point. In the SDW case, quasiparticles disintegrate only near hot spots, the parts of the Fermi surface that are connected by the antiferromagnetic wavevector. We have discussed how the non-Fermi liquid behavior intertwines with the additional modes of quantum criticality, and how this quantum critical behavior has been experimentally probed through observations that pertain to dynamical scaling, Fermi surface jump, extra energy scale and mass divergence.

The notion of Kondo destruction has also provided a means to characterize new quantum phases in antiferromagnetic heavy fermion metals. The resulting global phase diagram contains novel phases near the quantum critical points, that are not expected when the phases are only distinguished in terms of spontaneously broken symmetries as in the Landau framework. Experimental evidence is growing for the phases that are differentiated by both Fermi surfaces and magnetic order parameter. Furthermore, the global phase diagram is fueling the recent efforts to extend the basis of heavy fermion materials with varying dimensionality or frustration-enhanced quantum fluctuations.

These insights on the normal state will undoubtedly impact on our understanding of superconductivity in heavy fermion metals, which tends to occur near quantum critical points. The spin-density-wave quantum critical excitations provide the basis for the spin-fluctuation theory of heavy fermion superconductivity, which assumes that a large Fermi surface is fully formed and quasiparticles near the hot spots are coupled to the critical spin fluctuations. Given the considerable evidence for local quantum criticality, it will be important to theoretically address how superconducting pairing arises out of such a drastic non-Fermi liquid state.

The insights gained on these issues, regarding non-Fermi liquid behavior and unconventional superconductivity, will likely be relevant to the understanding of other strongly correlated electron systems. Several additional aspects of heavy fermion physics also promise to have implications in broader contexts. The development of local quantum criticality has taken place through the Kondo destruction physics in heavy fermion metals. As an interacting critical theory involving inherently quantum modes, it promises to connect with the physics of quantum phase transitions in other contexts. It has already influenced the development of quantum criticality in insulating magnets. More recently, tantalizing connections have been drawn between local quantum criticality in Kondo lattice systems and criticality emerging from holographic models in weakly curved anti-de Sitter (AdS) spacetime through the string/field theory duality [126,84,127]; “semi-local” critical points with closely related form of correlation functions have been constructed from the gravity side [128,129]. New insights are likely to come from exploring this connection further.

Recent efforts, both theoretical and experimental, were devoted to spin-orbit coupling and topological states in heavy fermion systems. When spin-orbit couplings are explicitly taken into account, the tuning among the Kondo insulator and antiferromagnetic states we discussed for the Kondo insulator systems would be generalized to the transformation among the topological and Kondo coherent/magnetic states. It is therefore likely that Kondo insulator systems will serve as a promising setting to study correlation effects on topological insulating states.

Acknowledgements We would like to thank many colleagues for collaborations and discussions, including E. Abrahams, P. Coleman, J. Custers, J. Dai, S. Friedemann, P. Gegenwart, C. Geibel, P. Goswami, K. Ingersent, S. Kirchner, C. Krellner, H. Liu, A. H. Nevidomskyy, E. Nica, J. Pixley, A. J. Schofield, F. Steglich, O. Stockert, A. M. Strydom, S. Wirth, J. Wu, S. Yamamoto, R. Yu, H. Q. Yuan, J.-X. Zhu, and L. Zhu. This work has been supported in part by the NSF Grant No. DMR-1006985, the Robert A. Welch Foundation Grant No. C-1411, and the European Research Council under the European Community’s Seventh Framework Programme (FP7/2007-2013)/ERC grant agreement no. 227378.

References

- [1] Focus issue: Quantum phase transitions. *Nature Phys.* **4**, 167-204 (2008).
- [2] Special issue: Quantum Phase Transitions. *J. Low Temp. Phys.* **161**, 1-323 (2010).
- [3] Q. Si and F. Steglich, *Science* **329**, 1161–1166 (2010).
- [4] H. v. Löhneysen, A. Rosch, M. Vojta, and P. Wölfle, *Rev. Mod. Phys.* **79**, 1015 (2007).
- [5] G. R. Stewart, *Rev. Mod. Phys.* **73**, 797–855 (2001).
- [6] A. C. Hewson, *The Kondo Problem to Heavy Fermions* (Cambridge University Press, Cambridge, 1993).
- [7] M. Klein, A. Nuber, F. Reinert, J. Kroha, O. Stockert, and H. v. Löhneysen, *Phys. Rev. Lett.* **101**, 266404 (2008).
- [8] S. Ernst, S. Kirchner, C. Krellner, C. Geibel, G. Zwicknagl, F. Steglich, and S. Wirth, *Nature* **474**, 362–366 (2011).
- [9] G. Aeppli and Z. Fisk, *Comments Condens. Matter Phys.* **16**, 155 (1992).
- [10] P. S. Riseborough, *Adv. Phys.* **49**, 257 (2000).
- [11] H. Tsunetsugu, M. Sigrist, and K. Ueda, *Rev. Mod. Phys.* **69**, 809 (1997).
- [12] S. Doniach, *Physica B* **91**, 231–234 (1977).
- [13] C. M. Varma, *Rev. Mod. Phys.* **48**, 219–238 (1976).
- [14] J. A. Hertz, *Phys. Rev. B* **14**, 1165–1184 (1976).
- [15] T. Moriya, *Spin Fluctuations in Itinerant Electron Magnetism* (Springer, Berlin, 1985).
- [16] A. J. Millis, *Phys. Rev. B* **48**, 7183–7196 (1993).
- [17] Q. Si and J. L. Smith, *Phys. Rev. Lett.* **77**, 3391 (1996).
- [18] J. L. Smith and Q. Si, *arXiv:cond-mat/9705140*, *Europhys. Lett.* **45**, 228 (1999).
- [19] A. M. Sengupta, *arXiv:cond-mat/9707316*, *Phys. Rev. B* **61**, 4041–4043 (2000).
- [20] Q. Si, J. L. Smith, and K. Ingersent, *Int. J. Mod. Phys. B* **13**, 2331 (1999).
- [21] A. Schröder, G. Aeppli, R. Coldea, M. Adams, O. Stockert, H. v. Löhneysen, E. Bucher, R. Ramazashvili, and P. Coleman, *Nature* **407**, 351–355 (2000).
- [22] Q. Si, S. Rabello, K. Ingersent, and J. Smith, *Nature* **413**, 804–808 (2001).
- [23] P. Coleman, C. Pépin, Q. Si, and R. Ramazashvili, *J. Phys. Cond. Matt.* **13**, R723 (2001).
- [24] Q. Si, S. Rabello, K. Ingersent, and J. Smith, *Phys. Rev. B* **68**, 115103 (2003).
- [25] T. Senthil, M. Vojta, and S. Sachdev, *Phys. Rev. B* **69**, 035111 (2004).
- [26] I. Paul, C. Pépin, and M. R. Norman, *Phys. Rev. Lett.* **98**, 026402 (2007).
- [27] L. D. Leo, M. Civelli, and G. Kotliar, *Phys. Rev. Lett.* **101**, 256404 (2008).
- [28] P. Wölfle and E. Abrahams, *Phys. Rev. B* **84**, 041101(R) (2011).
- [29] J. L. Smith and Q. Si, *Phys. Rev. B* **61**, 5184–5193 (2000).
- [30] R. Chitra and G. Kotliar, *Phys. Rev. Lett.* **84**, 3678–3681 (2000).
- [31] D. Grempel and Q. Si, *Phys. Rev. Lett.* **91**, 026401 (2003).
- [32] J. X. Zhu, S. Kirchner, R. Bulla, and Q. Si, *Phys. Rev. Lett.* **99**, 227204 (2007).
- [33] M. Glossop and K. Ingersent, *Phys. Rev. Lett.* **99**, 227203 (2007).
- [34] J. Zhu, D. Grempel, and Q. Si, *Phys. Rev. Lett.* **91**, 156404 (2003).
- [35] M. C. Aronson, R. Osborn, R. A. Robinson, J. W. Lynn, R. Chau, C. L. Seaman, and M. B. Maple, *Phys. Rev. Lett.* **75**, 725–728 (1995).
- [36] S. Friedemann, N. Oeschler, S. Wirth, C. Krellner, C. Geibel, F. Steglich, S. Paschen, S. Kirchner, and Q. Si, *PNAS* **107**, 14547–14551 (2010).
- [37] J. Custers, K. Lorenzer, M. Müller, A. Prokofiev, A. Sidorenko, H. Winkler, A. M. Strydom, Y. Shimura, T. Sakakibara, R. Yu, Q. Si, and S. Paschen, *Nature Mater.* **11**, 189 (2012).
- [38] S. Paschen, T. Lühmann, S. Wirth, P. Gegenwart, O. Trovarelli, C. Geibel, F. Steglich, P. Coleman, and Q. Si, *Nature* **432**, 881–885 (2004).

- [39] M. Lee, A. Husmann, T.F. Rosenbaum, and G. Aeppli, Phys. Rev. Lett. **92**, 187201 (2004).
- [40] R. Jaramillo, Y. Feng, J. Wang, and T.F. Rosenbaum, PNAS **107**, 13631 (2010).
- [41] S. Friedemann, N. Oeschler, S. Wirth, C. Krellner, C. Geibel, F. Steglich, S. Paschen, S. Kirchner, and Q. Si, J. Phys.: Condens. Matter **23**, 094216 (2011).
- [42] H. Shishido, R. Settai, H. Harima, and Y. Ōnuki, J. Phys. Soc. Jpn. **74**, 1103–1106 (2005).
- [43] T. Park, F. Ronning, H.Q. Yuan, M.B. Salamon, R. Movshovich, J.L. Sarrao, and J.D. Thompson, Nature **440**, 65–68 (2006).
- [44] G. Knebel, J. Buhot, D. Aoki, G. Lapertot, S. Raymond, E. Ressouche, and J. Flouquet, J. Phys. Soc. Jpn. **80**, SA001 (2011).
- [45] G. Knebel, D. Aoki, J.P. Brison, and J. Flouquet, J. Phys. Soc. Jpn. **77**, 114704–114717 (2008).
- [46] T. Lizuka, T. Mizuno, B.H. Min, Y.S. Kwon, and S. Kimura, J. Phys. Soc. Jpn. **81**, 043703 (2012).
- [47] G. Bossé, L.S. Bilbro, R.V. Aguilar, W.L. L. Pan, A.V. Stier, Y. Li, J. Eckstein, and N.P. Armitage, Phys. Rev. B **85**, 155105 (2012).
- [48] H. Pfau, S. Hartmann, U. Stockert, P. Sun, S. Lausberg, M. Brando, S. Friedemann, C. Krellner, C. Geibel, S. Wirth, S. Kirchner, E. Abrahams, Q. Si, and F. Steglich, Nature **484**, 493–497 (2012).
- [49] P. Aynajian, E.H. da Silva Neto, A. Gyenis, R.E. Baumbach, J.D. Thompson, Z. Fisk, E.D. Bauer, and A. Yazdani, Nature **486**, 201–206 (2012).
- [50] C. Stock, C. Broholm, F. Demmel, J. Van Duijn, J.W. Taylor, H.J. Kang, R. Hu, and C. Petrovic, Phys. Rev. Lett. **109**, 127201 (2012).
- [51] Q. Si, Physica B **378**, 23–27 (2006).
- [52] Q. Si, Phys. Status Solidi B **247**, 476–484 (2010).
- [53] P. Coleman and A. Nevidomskyy, J. Low Temp. Phys. **161**, 182–202 (2010).
- [54] S. Yamamoto and Q. Si, Phys. Rev. Lett. **99**, 016401 (2007).
- [55] P. Goswami and Q. Si, Phys. Rev. Lett. **107**, 126404 (2011).
- [56] S. Friedemann, T. Westerkamp, M. Brando, N. Oeschler, S. Wirth, P. Gegenwart, C. Krellner, C. Geibel, and F. Steglich, Nat. Phys. **5**, 465–469 (2009).
- [57] J. Custers, P. Gegenwart, C. Geibel, F. Steglich, P. Coleman, and S. Paschen, Phys. Rev. Lett. **104**, 186402 (2010).
- [58] Y. Tokiwa, P. Gegenwart, C. Geibel, and F. Steglich, J. Phys. Soc. Jpn. **78**, 123708 (2009).
- [59] Y. Tokiwa and P.G. et al., work presented at QCNP12.
- [60] S.E. Sebastian, N. Harrison, C.D. Batista, S.A. Trugman, V. Fanelli, M. Jaime, T.P. Murphy, E.C. Palm, H. Harima, and T. Ebihara, PNAS **106**, 7741–7744 (2009).
- [61] H. Shishido, T. Shibauchi, K. Yasu, T. Kato, H. Kontani, T. Terashima, and Y. Matsuda, Science **327**, 980–983 (2010).
- [62] Y. Mizukami, H. Shishido, T. Shibauchi, M. Shimozaawa, S. Yasumoto, D. Watanabe, M. Yamashita, H. Ikeda, T. Terashima, H. Kontani, and Y. Matsuda, Nat. Phys. **7**, 849 (2011).
- [63] S. Bud'ko, V. Zapf, E. Morosan, and P. Canfield, Phys. Rev. B **72**, 172413 (2005).
- [64] M.S. Kim and M.C. Aronson, Phys. Rev. Lett. **110**, 017201 (2013).
- [65] E.D. Mun, S.L. Bud'ko, C. Martin, H. Kim, M.A. Tanatar, J.H. Park, T. Murphy, G.M. Schmiedeshoff, N. Dilley, R. Prozorov, and P.C. Canfield, Magnetic field tuned quantum criticality of heavy fermion system YbPtBi, arXiv:1211.0636.
- [66] V. Fritsch, N. Bagrets, G. Goll, W. Kittler, M.J. Wolf, K. Grube, C.L. Huang, and H. v. Löhneysen, Quantum criticality in a partially geometrically frustrated heavy-fermion system: $CePd_{1-x}Ni_xAl$, arXiv:1301.6062.
- [67] H. Hegger, C. Petrovic, E.G. Moshopoulou, M.F. Hundley, J.L. Sarrao, Z. Fisk, and J.D. Thompson, Phys. Rev. Lett. **84**, 4986–4989 (2000).
- [68] M. Okawa, M. Matsunami, K. Ishizaka, R. Eguchi, M. Taguchi, A. Chainani, Y. Takata, M. Yabashi, K. Tamasaku, Y. Nishino, T. Ishikawa, K. Kuga, N. Horie, S. Nakatsuji, and S. Shin, Phys. Rev. Lett. **104**, 247201 (2010).
- [69] P. Wachter, Handbook of the Physics and Chemistry of Rare Earths, (North-Holland, Amsterdam, 1994), pp. 177, Vol. 19.
- [70] A. Menth, E. Buehler, and T.H. Geballe, Phys. Rev. Lett. **22**, 295 (1969).
- [71] E.E. Vanstein, S.M. Blokhin, and Y.B. Paderno, Sov. Phys. Solid State **6**, 281 (1965).
- [72] L.M. Falicov and J.C. Kimball, Phys. Rev. Lett. **22**, 997–999 (1969).
- [73] Q. Si and G. Kotliar, Phys. Rev. B **48**, 13881–13903 (1993).
- [74] I.E. Perakis, C.M. Varma, and A.E. Ruckenstein, Phys. Rev. Lett. **70**, 3467–3470 (1993).
- [75] Q. Si, J. Phys.: Condens. Matter **8**, 9953–9984 (1996).
- [76] S. Watanabe and K. Miyake, Phys. Rev. Lett. **105**, 186403 (2010).
- [77] S. Watanabe and K. Miyake, J. Phys. Soc. Jpn. **79**, 033707 (2010).
- [78] S. Watanabe and K. Miyake, J. Phys.: Condens. Matter **24**, 294208 (2012).
- [79] J.H. Pixley, S. Kirchner, K. Ingersent, and Q. Si, Phys. Rev. Lett. **109**, 086403 (2012).
- [80] L. Zhu, M. Garst, A. Rosch, and Q. Si, Phys. Rev. Lett. **91**, 066404 (2003).
- [81] J. Wu, L. Zhu, and Q. Si, J. Phys.: Conf. Series **273**, 012019 (2011).
- [82] Y. Matsumoto, S. Nakatsuji, K. Kuga, Y. Karaki, N. Horie, Y. Shimura, T. Sakakibara, A.H. Nevidomskyy, and P. Coleman, Science **331**, 316–319 (2011).
- [83] S. Nakatsuji, K. Kuga, Y. Machida, T. Tayama, T. Sakakibara, Y. Karaki, H. Ishimoto, S. Yonezawa, Y. Maeno, E. Pearson, G. Lonzarich, L. Balicas, H. Lee, and Z. Fisk, Nature Phys. **4**, 603 (2008).
- [84] S.J. Yamamoto and Q. Si, J. Low Temp. Phys. **161**, 233 (2010).
- [85] J. Cooley, C. Mielke, V. Hults, J. Goettee, M. Honold, R. Modler, A. Lacerda, D. Rickel, and J. Smith, J. Supercond. **12**, 171 (1999).

- [86] M. Jaime, R. Movshovich, G. Stewart, W. Beyersmann, M. Berisso, M. Hundley, P. Canfield, and J. Sarrao, *Nature* **405**, 160 (2000).
- [87] B. Buschinger, M. Weiden, O. Trovarelli, P. Hellmann, C. Geibel, and F. Steglich, *J. Phys.: Condens. Matter* **10**, 2021 (1998).
- [88] G.M. Kalvius, A. Kratzer, G. Grosse, D.R. Noakes, R. Wäppling, H. v. Löhneysen, T. Takabatake, and Y. Echizen, *Physica B* **289&290**, 256 (2000).
- [89] A. Slebarski and J. Spalek, *Phys. Rev. Lett.* **95**, 046402 (2005).
- [90] N.E. Sluchanko, A.N. Azarevich, A.V. Bogach, V.V. Glushkov, S.V. Demishev, M.A. Anisimov, A.V. Levchenko, V.B. Filipov, and N.Y. Shitsevalova, *JETP* **115**, 509 (2012).
- [91] A. Barla, J. Derr, J. P. Sanchez, B. Salce, G. Lapertot, B. P. Doyle, R. Rüffer, R. Lengsdorf, M.M. Abd-Elmeguid, and J. Flouquet, *Phys. Rev. Lett.* **94**(Apr), 166401 (2005).
- [92] M. Kasaya, T. Tani, F. Iga, and T. Kasuya, *J. Magn. Magn. Mater.* **76&77**, 278 (1988).
- [93] S. K. Malik, D. T. Adroja, S. K. Dhar, R. Vijayaraghavan, and B. D. Padalia, *Phys. Rev. B* **40**, 2414 (1989).
- [94] D. T. Adroja and B. D. Rainford, *Physica B* **194-196**, 363 (1994).
- [95] J. Sakurai, R. Kawamura, T. Taniguchi, S. Nishigori, S. Ikeda, H. Goshima, T. Suzuki, and T. Fujita, *J. Magn. Magn. Mater.* **104-107**, 1415 (1992).
- [96] D. T. Adroja, B. D. Rainford, A. J. Neville, and A. G. M. Jansen, *Physica B* **223&224**, 275 (1996).
- [97] M. Kasaya, T. Tani, H. Suzuki, K. Ohoyama, and M. Kohgi, *J. Phys. Soc. Jpn.* **60**, 2542 (1991).
- [98] J. Sánchez Marcos, J. Rodríguez Fernández, and B. Chevalier, *J. Magn. Magn. Mater.* **310**, 383 (2007).
- [99] F. Iga, M. Kasaya, H. Suzuki, Y. Okayama, H. Takahashi, and N. Mori, *Physica B* **186 -188**, 419 (1993).
- [100] A. M. Alsmadi, M. S. Torikachvili, M. K. Kothapalli, F. Nasreen, and H. Nakotte, *J. Phys.: Conf. Series* **273**, 012025 (2011).
- [101] A. M. Strydom, *Physica B* **404**, 2981–2984 (2009).
- [102] M. Z. Hasan and C. L. Kane, *Rev. Mod. Phys.* **82**, 3045–3067 (2010).
- [103] X. L. Qi and S. C. Zhang, *Rev. Mod. Phys.* **83**, 1057–1110 (2011).
- [104] M. Dzero, K. Sun, V. Galitski, and P. Coleman, *Phys. Rev. Lett.* **104**, 106408 (2010).
- [105] X. Y. Feng, J. Dai, C. H. Chung, and Q. Si, Competing topological and Kondo insulator phases on a honeycomb lattice, arXiv:1206.0979.
- [106] S. Wolgast, C. Kurdak, K. Sun, J. W. Allen, D. J. Kim, and Z. Fisk, Discovery of the first topological Kondo insulator: Samarium Hexaboride, arXiv:1211.5104.
- [107] J. Botimer, D. J. Kim, S. Thomas, T. Grant, Z. Fisk, and J. Xia, Robust surface Hall effect and nonlocal transport in SmB₆: Indication for an ideal topological insulator, arXiv:1211.6769.
- [108] D. Belitz, T. R. Kirkpatrick, and T. Vojta, *Rev. Mod. Phys.* **77**, 579–632 (2005).
- [109] M. Uhlarz, C. Pfleiderer, and S. M. Hayden, *Phys. Rev. Lett.* **93**, 256404 (2004).
- [110] S. J. Yamamoto and Q. Si, *PNAS* **107**, 15704–15707 (2010).
- [111] C. A. King and G. G. Lonzarich, *Physica B* **171**, 161–165 (1991).
- [112] N. P. Butch and M. B. Maple, *Phys. Rev. Lett.* **103**, 076404 (2009).
- [113] R. E. Baumbach, H. Chudo, H. Yasuoka, F. Ronning, E. D. Bauer, and J. D. Thompson, *Phys. Rev. B* **85**, 094422 (2012).
- [114] R. Miyazaki, Y. Aoki, R. Higashinaka, H. Sato, T. Yamashita, and S. Ohara, *Phys. Rev. B* **86**, 155106 (2012).
- [115] C. Krellner, S. Lausberg, A. Steppke, M. Brando, L. Pedrero, H. Pfau, S. Tencé, H. Rosner, F. Steglich, and C. Geibel, *New J. Phys.* **13**, 103014 (2011).
- [116] S. Kitagawa, K. Ishida, T. Nakamura, M. Matoba, and Y. Kamihara, *Phys. Rev. Lett.* **109**, 227004 (2012).
- [117] P. C. Ho, N. A. Frederick, V. S. Zapf, E. D. Bauer, T. D. Do, M. B. Maple, A. D. Christianson, and A. H. Lacerda, *Phys. Rev. B* **67**, 180508 (2003).
- [118] H. C. Walker, K. A. McEwen, E. Colineau, J. Griveau, and F. Wastin, *J. Magn. Magn. Mater.* **310**, 751 (2007).
- [119] E. Miranda and V. Dobrosavljević, *Rep. Progr. Phys.* **68**, 2337–2408 (2005).
- [120] A. H. C. Neto and B. A. Jones, *Phys. Rev. B* **62**, 14975–15011 (2000).
- [121] N. D. Mathur, F. M. Grosche, S. R. Julian, I. R. Walker, D. M. Freye, R. K. W. Haselwimmer, and G. G. Lonzarich, *Nature* **394**, 39–43 (1998).
- [122] A. W. Rost, R. S. Perry, J. F. Mercure, A. P. Mackenzie, and S. A. Grigera, *Science* **325**, 1360 – 1363 (2009).
- [123] V. A. Sidorov, E. D. Bauer, N. A. Frederick, J. R. Jeffries, S. Nakatsuji, N. O. Moreno, J. D. Thompson, M. B. Maple, and Z. Fisk, *Phys. Rev. B* **67**, 224419 (2003).
- [124] O. Stockert, J. Arndt, E. Faulhaber, C. Geibel, H. S. Jeevan, S. Kirchner, M. Loewenhaupt, K. Schmalzl, W. Schmidt, Q. Si, and F. Steglich, *Nat. Phys.* **7**, 119–124 (2011).
- [125] O. Stockert, S. Kirchner, F. Steglich, and Q. Si, *J. Phys. Soc. Jpn.* **81**, 011001 (2012).
- [126] N. Iqbal, H. Liu, M. Mezei, and Q. Si, *Phys. Rev. D* **82**, 045002 (2010).
- [127] S. Sachdev, *Phys. Rev. Lett.* **105**, 151602 (2010).
- [128] N. Iqbal, H. Liu, and M. Mezei, arXiv:1108.0425 (2011).
- [129] T. Faulkner, G. T. Horowitz, and M. M. Roberts, arXiv:1008.1581, JHEP04:051 (2011).